^{16}O Excesses in Olivine Inclusions in Yamato-86009 and Murchison Chondrites and Their Relation to CAIs

Hajime Hiyagon[1]* and Akihiko Hashimoto[2]

In situ ion microprobe analyses of oxygen isotopes in Yamato-86009 and Murchison chondrites show that they contain abundant olivine-rich inclusions that have large oxygen-16 (^{16}O) excesses, similar to those in spinel grains in calcium-aluminium–rich inclusions in Allende and other carbonaceous chondrites. The existence of ^{16}O-enriched olivine-rich inclusions suggests that oxygen isotopic anomalies were more extensive in the early solar system than was previously thought and that their origin may be attributed to a nebular chemical process rather than to an unidentified ^{16}O-rich carrier of presolar origin.

Calcium-aluminium–rich inclusions (CAIs), most commonly observed in carbonaceous chondrite groups (CV, CO, and CM chondrites), have anomalous oxygen isotopic compositions, with $\delta^{17}O$ and $\delta^{18}O$ values down to ~ -40 per mil (‰) (*1–3*) relative to the standard mean ocean water (SMOW) $\delta^{17}O$ and $\delta^{18}O$ values (*4*). The origin of these isotopic anomalies, however, is still under debate—whether they are derived from a carrier having extreme oxygen isotopic compositions (almost pure ^{16}O) (*1, 5*) or from mass-independent fractionation caused by some kind of chemical process (*6–9*). It has generally been considered that such oxygen isotopic anomalies are characteristic of highly refractory components (CAIs) and not of less refractory Mg-rich ones, although some olivine phases rarely observed inside CAIs are found to have relatively high oxygen isotopic anomalies (*10*). In the course of our in situ ion microprobe study of oxygen isotopes, however, we discovered abundant olivine-rich inclusions (OIs) in two chondrites that have excess ^{16}O, with $\delta^{17}O$ and $\delta^{18}O$ values down to ~ -50‰, which is similar to the highest anomalies observed in Allende and Murchison CAIs (*2, 3*). We report here details of our findings and discuss the origin of the oxygen isotopic anomalies on the basis of our results.

Recent improvements in ion microprobe techniques have enabled in situ analyses of oxygen isotopes with a spatial resolution of ~ 10 μm and a precision of ~ 1‰ (*11*). These technical improvements allow us to study the micro-distribution of oxygen isotopes in different components in meteorites, which is essential to understanding the origin of the oxygen isotopic anomalies. We performed in situ oxygen isotope analyses of Yamato-86009 (CV3) and Murchison (CM2) chondrites using a CAMECA ims-6f ion microprobe. A Cs^+ primary beam ~ 15 μm in diameter, with a beam intensity of 0.1 to 0.3 nA and an impact energy of 19.5 kV, was used for the analyses (except for position 19; see Table 1). Negative ions of oxygen isotopes were accelerated at −9.5 kV, separated at a mass resolution of ~5000, and detected with a Faraday Cup ($^{16}O^-$) or an electron-multiplier–based ion counting system ($^{17}O^-$, $^{16}O^1H^-$, and $^{18}O^-$). The contribution of the $^{16}O^1H^-$ peak was negligible ($\ll 1$‰) at the center of the $^{17}O^-$ peak for all the analyses. A normal incidence electron gun was used for charge compensation. Repeated analyses were performed on a San Carlos olivine standard (*12*) before and after the periods of sample analyses without changing the analytical conditions, and all the data were normalized to the average of the San Carlos olivine data. The reproducibility of the analysis was $\sim \pm 1.5$‰ for $^{17}O/^{16}O$ and $\sim \pm 2.2$‰ for $^{18}O/^{16}O$ (1σ) for all analyses.

The meteorite samples were prepared in thin sections, carbon-coated, examined with a scanning electron microscope (SEM) equipped with an energy-dispersive x-ray spectrometer (EDS) for petrographic studies, and used for the ion microprobe analysis. We selected four OIs from Yamato-86009 (Y86009-A, -B, -C, and -D) and four OIs from Murchison (MC5a-26, -47, -52, and -94) for the ion microprobe analysis. The OIs are composed predominantly of Mg-rich olivine (Table 1) and of variable amounts (~ 1 to ~50% by volume) of interspersed Ca-Al–rich domains (mostly diopsidic or fassaitic pyroxene with or without spinel) enclosed by the olivine. The OIs are irregular but lumpy in shape, and many of them have numerous irregularly shaped voids (typically submicrometer sized to a few micrometers in diameter) both in olivine and in Ca-Al–rich phases (Fig. 1) (*13*). The irregular shape of the OIs and the voids suggests that OIs never completely melted but formed by the sintering of small forsterite grains at subsolidus temperatures. The typical size of OIs is 50 to 200 μm, but some exceed 300 μm and they occupy more than 1% by volume of these meteorites (*14*).

For comparison, one CAI (Y86009-E) and one chondrule (Y86009-F) in Yamato-86009 and one chondrule (MC5a-85) in Murchison were also analyzed. Y86009-E is a spinel-pyroxene-feldspar aggregate (*15*). Because of its fine-grained texture (typical grain size <20 μm), individual phases could not be analyzed without some overlap to other phases, except for one spinel grain (position 12). Y86009-F (~900 μm in diameter) consists of enstatite, forsterite (rounded grains of 10 to 50 μm in size, poikilitically enclosed by enstatite), diopside (euhedral crystals rimming enstatite and protruding into the glass), and glass. MC5a-85 (~100 μm by ~170 μm in size) consists predominantly of enstatite and forsterite with minor (less than a few percent) amounts of diopside and ferrosilite.

All 13 analyses on olivine grains inside eight OIs showed ^{16}O enrichments with $\delta^{17}O$ and $\delta^{18}O$ ranging from ~ -42 to ~ -51‰. (One datum for position 23 is omitted from the discussion because of its large errors, caused by the instability of the secondary ion beam.) Ca-Al–rich phases in Yamato-86009 OIs showed relatively smaller ^{16}O enrichments with $\delta^{17}O$ and $\delta^{18}O$ ranging from ~ -32 to ~ -42‰. Spinel and spinel-rich phases of the CAI (Y86009-E) exhibited ^{16}O enrichments with $\delta^{17}O$ and $\delta^{18}O$ ranging from ~ -41 to ~ -49‰, which are consistent with the previous results for spinel in Allende and Murchison (*2, 3*). The two chondrules (Y86009-F and MC5a-85) exhibited much smaller oxygen isotopic anomalies, with $\delta^{17}O$ and $\delta^{18}O$ ranging from ~ -13 to ~ -4‰ (*16*).

It is known that physical and chemical processes such as evaporation, condensation, diffusion, and chemical reactions in general, accompany mass-dependent isotopic fractionations. Oxygen is highly mobile in many circumstances in nature and is expected to show large isotopic fractionations. If isotopic compositions of oxygen in both the start and end materials generated in those processes are expressed in the so-called three-isotope diagram (Fig. 2), they should form a line, with slope ~1/2, according to the mass differences for the ^{17}O-^{16}O pair (one mass unit) and the ^{18}O-^{16}O pair (two mass units). An example is the terrestrial fractionation (TF) line for terrestrial materials. Mineral separates from CAIs in Allende and other carbonaceous chondrites, on the other hand, form a correlation line

---

[1] Department of Earth and Planetary Physics, University of Tokyo, Bunkyo-ku, Tokyo 113-0033, Japan. [2] Department of the Earth and Planetary Sciences, Hokkaido University, Sapporo 060-0810, Japan.

*To whom correspondence should be addressed. E-mail: hiyagon@geoph.s.u-tokyo.ac.jp

with slope ~1 called carbonaceous chondrite anhydrous mineral (CCAM) line. They exhibit up to 4 to 5% (or 40 to 50‰) of ^{16}O enrichments relative to SMOW, which is much different from the bulk isotopic compositions of most of the solar system materials (meteorites, Earth, the moon, and Mars; see the insert in Fig. 2). The CCAM line (or any correlation line with a slope different from 1/2) is inexplicable by the processes that accompany a mass-dependent isotope fractionation. The correlation line with slope ~1 may require mixing of an isotopically distinct ^{16}O-rich material that has an isotopic composition along the lower left extension of the line, to an isotopically "normal" oxygen reservoir with an oxygen isotopic composition located somewhere on the upper right extension. Alternatively, an extraordinary chemical reaction may have enacted mass-independent fractionation of oxygen isotopes in the solar nebula (*6–9*). The fact that OIs, like spinel in CAIs, plot in the lower end of the CCAM line suggests a common oxygen source or a similar chemical process for both OIs and CAIs.

The discovery that isotopically anomalous OIs are abundantly present in the two chondrite thin sections (*14*) demonstrates that the oxygen isotopic anomalies with $\delta^{17}O$ and $\delta^{18}O$ ranging from ~−40 to ~−50‰ are characteristic not only of Ca-Al–rich components but also of the most common meteoritic and planetary silicate (olivine), implying that such oxygen isotopic anomalies were rather extensive in the early solar system. In terms of the mineral stability relationships applied to the nebulae (*17*), forsterite has a high condensation temperature among other condensable phases, except for the CAI minerals such as spinel and gehlenite, which have higher condensation temperatures than that of forsterite. The less refractory nature of OIs as compared to CAIs suggests that the largest oxygen isotopic anomalies (~−50‰) are not limited to the highest temperature conden-

Table 1. Analyzed phases and their oxygen isotopic compositions. Ag, spinel-pyroxene-feldspar aggregate; Ch, chondrule.

Inclusion no.	Position no.	Minerals	Mg#*	$\delta^{18}O$ (‰)†	$\delta^{17}O$ (‰)†
Yamato-86009 (CV3)					
Y86009-A OI	1	Forsterite	98.8–99.7	−47.9 ± 2.3	−49.8 ± 1.8
	2	Forsterite	99.2–99.8	−46.0 ± 2.5	−46.5 ± 1.9
	3	Fassaite		−31.6 ± 2.4	−35.3 ± 1.9
	4	Diopside + spinel + forsterite		−40.4 ± 2.3	−41.6 ± 1.8
	5	Forsterite (+diopside)	99.3–99.8	−51.0 ± 2.5	−49.7 ± 1.8
Y86009-B OI	6	Forsterite	96.2–98.7	−49.1 ± 2.5	−49.8 ± 2.0
	7	Forsterite	95.2–98.2	−45.2 ± 2.4	−47.0 ± 1.8
	8	Forsterite	96.4–98.3	−45.8 ± 2.4	−46.2 ± 1.9
Y86009-C OI	9	Forsterite (+diopside)	99.4–99.6	−44.5 ± 2.3	−42.5 ± 1.8
Y86009-D OI	10	Forsterite	95.6–98.4‡	−46.1 ± 2.3	−46.8 ± 1.8
	11	Fassaite		−35.5 ± 2.4	−38.4 ± 1.9
Y86009-E Ag	12	Spinel		−49.3 ± 2.4	−48.3 ± 1.9
				−42.2 ± 2.3	−47.6 ± 1.9
	13	Spinel + fassaite		−41.2 ± 2.5	−42.1 ± 2.0
				−41.5 ± 2.5	−42.1 ± 1.9
	14	Mix (feldspar + spinel)		−12.3 ± 2.5	−15.0 ± 2.0
	15	Mix (feldspar-rich)		6.4 ± 2.4	0.5 ± 1.8
	16	Mix (feldspar-rich)		6.5 ± 2.4	−1.5 ± 1.8
	17	Mix (feldspar-rich)		8.0 ± 2.9	2.1 ± 2.1
	18	Mix (pyroxene-rich)		−12.9 ± 2.5	−14.9 ± 2.0
Y86009-F Ch	19	Forsterite	99.3	−6.1 ± 2.5§	−10.6 ± 1.9§
	20	Forsterite	99.3	−6.8 ± 2.5	−12.8 ± 2.0
	21	Enstatite	99.1	−11.4 ± 2.6	−12.7 ± 1.9
	22	Diopside		−5.5 ± 2.3	−8.6 ± 1.8
Murchison (CM2)					
MC5a-52 OI	23	Forsterite	99.8	−57.3 ± 5.3‖	−51.7 ± 2.3‖
	24	Forsterite	99.1–99.7	−45.7 ± 2.3	−47.7 ± 1.9
MC5a-47 OI	25	Forsterite	99.8	−46.8 ± 2.3	−44.8 ± 1.9
MC5a-26 OI	26	Forsterite	99.5–99.6	−47.4 ± 2.3	−47.7 ± 1.9
MC5a-94 OI	27	Forsterite	99.7	−46.6 ± 2.2	−47.1 ± 1.8
MC5a-85 Ch	28	Enstatite	98.5–98.7	−8.1 ± 2.3	−10.7 ± 1.9
	29	Enstatite	98.5–98.7	−4.0 ± 2.3	−7.1 ± 1.8

*Mg# = Mg/(Mg + Fe) [mol %]. †Errors are 1σ. ‡A small amount of iron-rich phase exists with Mg# = 75 to 80. §Measured with a Cs^+ primary beam ~30 μm in diameter and ~0.4 nA of beam intensity. ‖The beam was unstable for an unknown reason; large instrumental fractionation was suspected.

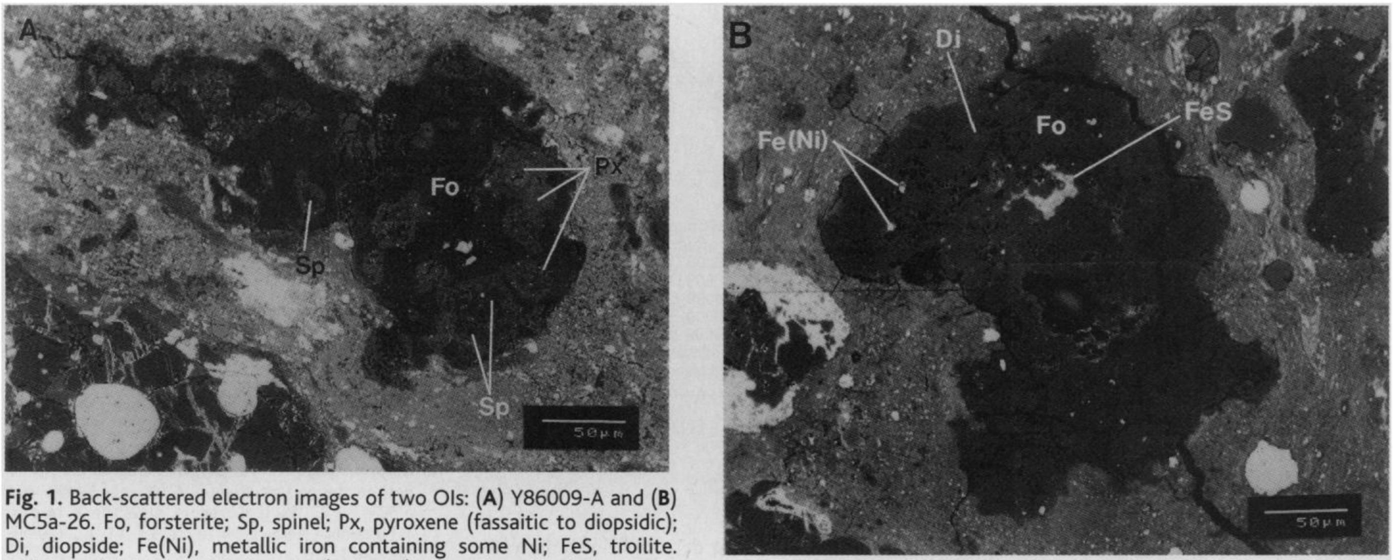

Fig. 1. Back-scattered electron images of two OIs: (**A**) Y86009-A and (**B**) MC5a-26. Fo, forsterite; Sp, spinel; Px, pyroxene (fassaitic to diopsidic); Di, diopside; Fe(Ni), metallic iron containing some Ni; FeS, troilite. Calcium-aluminium–rich domains (Px + Sp) are enclosed by forsterite in Y86009-A. Many irregularly shaped voids (typically less than a few micrometers) and a large void in the center are visible in MC5a-26. This OI contains only a small amount (~1 volume %) of diopside grains less than a few micrometers in size, interspersed in forsterite.

sates. Yet its refractory nature compared to the rest of the condensable phases reinforces a previously held view that the oxygen isotopic anomalies are somehow linked to high temperatures.

A presolar component model, in which a carrier (seed crystals) of an ^{16}O-rich oxygen (almost pure ^{16}O) is assumed, has been one of the preferred models for the origin of the oxygen isotope anomalies in CAIs. In this model, the ^{16}O-enriched refractory oxide grains of presolar origin provided nucleation sites for CAI-forming minerals to condense from a hot nebular gas (*1, 18*). However, such a model cannot explain the present observations. After the condensation of CAIs, the seed crystals would disappear before forsterite condensed. Even if they survived, forsterite would have to incorporate them in exactly the same dilution as for the CAIs to explain the unique $\delta^{17}O$ and $\delta^{18}O$ values (namely, −40 to −50‰). In fact, presolar oxides are rare (using current recovery procedures), and most do not show ^{16}O excesses (*19*) except for one oxide grain (~0.5 μm in diameter) discovered recently (*20*) in the Tieschitz ordinary chondrite. It has an extreme ^{16}O enrichment, but the inferred abundance of such grains [<0.25 part per billion (ppb)] in the meteorite is too low for them to be plausible carriers of ^{16}O enrichments in CAIs.

Further evidence against the presolar component model comes from recent discoveries of large oxygen isotopic anomalies ($\delta^{17}O$ and $\delta^{18}O$ down to ~−45‰) in diopside (*21*) in the Wark-Lovering rims (*22*) and in olivine (*23*) in accretionary rims (*19*) of CAIs. Because the Wark-Lovering rims and accretionary rims are considered to be features added later to main CAI bodies (*22, 24*), the observations that the cores and rims of CAIs have similar oxygen isotopic anomalies are difficult to reconcile with the idea of ^{16}O-rich, refractory seed crystals of presolar origin.

From another angle, the longtime effort by many researchers to characterize the isotopic signatures of CAIs, chondrules, and bulk chondrites has revealed that all the other elements do not show major mass-independent shifts from their canonical isotopic compositions when oxygen gives ~−40‰ variation from the terrestrial ensemble. This would appear to exclude a nucleosynthetic source for the ^{16}O excess in CAIs and OIs.

Alternatively, some particular sorts of chemical processes may have generated mass-independent isotopic fractionations before, during, or after the formation of these objects. Thiemens (*8*) argues that a mass-independent isotopic fractionation effect is restricted neither to ozone (O_3)-oxygen (O_2) reactions nor to photochemical reactions but should occur more generally. He postulated the possibilities of three different types of reactions: recombination reactions, isotopic exchange, and thermal dissociation. For example, Wen and Thiemens (*7*) have experimentally demonstrated that atomic oxygen was enriched in ^{16}O up to ~40‰ relative to CO_2 through isotopic exchange between the two gaseous species. This particular process, however, is unlikely to be a cause of the oxygen isotopic anomalies in CAIs or OIs because atomic oxygen and CO_2 are extremely minor constituents (*25*) as compared with the major oxygen-bearing gaseous species (such as CO and H_2O), which prevents their becoming effective oxygen reservoirs. Furthermore, in order to explain the oxygen isotopic anomalies in the condensed phases such as CAIs or OIs, the anomaly in the gas phase would have to be transferred into the lattice-forming oxygen; no effective process for this has been postulated.

We cannot presently determine the origin of the oxygen isotopic anomalies in CAIs and OIs. However, the observation that OIs, CAIs, and CAI rims all show a unique oxygen isotopic composition ($\delta^{17}O$ and $\delta^{18}O$ ~−40 to −50‰) seems to suggest that the oxygen isotopic anomalies are more plausibly attributed to some kind of nebular chemical process that occurred during the formation of these primordial objects rather than to an exotic carrier with ^{16}O enrichment.

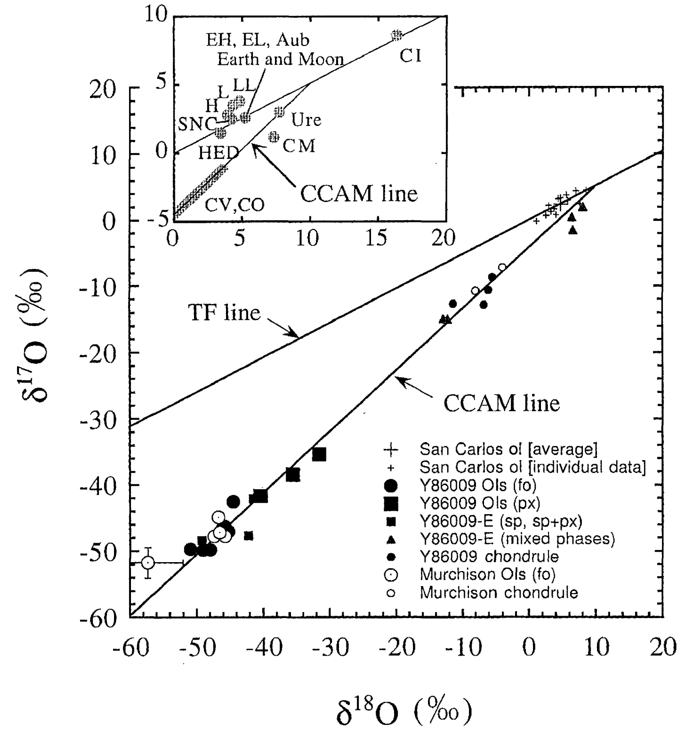

Fig. 2. Oxygen isotopic compositions of various phases in Yamato-86009 and Murchison chondrites. Also plotted for comparison (insert) are bulk oxygen isotopic compositions of different classes of meteorites and Earth and moon rocks (*26*). H, L, and LL, ordinary chondrites; CI, CM, CO, and CV, carbonaceous chondrites; HED, a class of differentiated meteorites (howardite, eucrite, and diogenite); SNC, martian meteorites; Ure, ureilite; EL and EH, enstatite chondrites; Aub, aubrite; TF line, terrestrial fractionation line (which has a slope of ~0.5); CCAM line, carbonaceous chondrite anhydrous mineral line, defined by many analyses of Allende CAI minerals (*2, 3*). All the Murchison and Yamato-86009 data are normalized to the average of San Carlos (SC) olivine data. Individual data for SC olivine are also shown after normalization to their average, demonstrating the reproducibility of the present ion microprobe analyses. Error bars are not shown except for position 23 for clarity. The definition of $\delta^{m}O$ is given in (*4*).

References and Notes

1. R. N. Clayton, L. Grossman, T. K. Mayeda, *Science* **182**, 485 (1973).
2. R. N. Clayton, N. Onuma, L. Grossman, T. K. Mayeda, *Earth Planet. Sci. Lett.* **34**, 209 (1977).
3. R. N. Clayton and T. K. Mayeda, *ibid.* **67**, 151 (1984).
4. $\delta^{m}O = [(^{m}O/^{16}O)_{sample}/(^{m}O/^{16}O)_{SMOW} - 1] \times 1000$ (‰), where m = 17 or 18 [H. Craig, *Science* **133**, 1833 (1961)].
5. J. M. Lattimer, D. N. Schramm, L. Grossman, *Astrophys. J.* **219**, 230 (1978).
6. M. H. Thiemens and J. E. Heidenreich III, *Science* **219**, 1073 (1983).
7. J. Wen and M. H. Thiemens, *J. Geophys. Res.* **98**, 12801 (1993).
8. M. H. Thiemens, in *Chondrules and the Protoplanetary Disk*, R. Hewins, R. H. Jones, E. R. D. Scott, Eds. (Cambridge Univ. Press, Cambridge, 1996), pp. 107–108.
9. A. Hashimoto and T. Takahashi, *Antarctic Meteorites* **22**, 49 (abstr.) (1997) (22nd Symposium on Antarctic Metorites, National Institute of Polar Research, Tokyo, 10 to 12 June 1997).
10. Clayton *et al.* (*2*) reported an olivine-rich separate (density 3.12 to 3.26 g/cm³) from an Allende inclusion (Al6S3) having a high oxygen isotopic anomaly with $\delta^{17}O = -34.3$‰ and $\delta^{18}O = -36.3$‰. M. Kimura *et al.* [*Geochim. Cosmochim. Acta* **57**, 2329 (1993)] reported forsteritic olivine with $\delta^{17}O = -34.6 \pm 6.1$‰ and $\delta^{18}O = -38.3 \pm 5.3$‰ separated from a CAI in a unique chondrite, ALH85085. Recently, Saxton *et al.* [J. M. Saxton, I. C. Lee, G. Turner, *Meteorit. Planet. Sci.* **33**, 1017 (1998)] reported relatively ^{16}O-rich olivine grains with $\delta^{18}O$ down to ~−10‰ from an ordinary chondrite Julesburg.
11. H. Hiyagon, *Antarctic Meteorite Res.* **10**, 249 (1997).
12. Isotopic composition of oxygen in San Carlos olivine used in the present study is $\delta^{17}O = +2.44$‰ and $\delta^{18}O = +4.70$‰ [I. Jabeen, M. Kusakabe, K. Nagao, T. Nakamura, *Antarct. Meteorite Res.* **11**, 122 (1998); see also (*11*)].
13. There are some similarities in mineralogy among OIs, olivine-pyroxene inclusions (OPIs) [G. J. MacPherson *et al.*, *Proc. Lunar Planet. Sci. Conf.* **15**, *J. Geophys.*

Res. Suppl. **89**, C299 (1984)], spinel-pyroxene-olivine inclusions (SPOIs) [R. C. Greenwood *et al.*, *Geochim. Cosmochim. Acta* **58**, 1913 (1994)], and amoeboid olivine aggregates (AOAs) [L. Grossman and I. M. Steel *ibid.* **40**, 149 (1976)]. However, OIs are made predominantly of forsterite, unlike OPIs and SPOIs. OIs resemble Allende AOAs in their high olivine proportions but are much more compact than the latter. OIs and AOAs [A. Hashimoto and L. Grossman, *ibid.* **51**, 1685 (1987)] are clearly distinguished from CAIs in mineral proportions, textures, chemistry, and overall morphologies.

14. Careful SEM-EDS observations suggest that at least 15 and 40 OIs of similar morphologies are present in the thin sections of Y-86009 (5 mm by 5 mm) and Murchison (6 mm by 7.5 mm), respectively, which suggests that OIs are rather abundant in these meteorites. In fact, the four Murchison OIs studied here were randomly chosen from more than 40 OIs that we had recognized before the ion microprobe analyses, and all of them were found to have large oxygen isotopic anomalies.
15. Pyroxene is fassaitic to diopsidic in composition with variable aluminum content. Feldspathic phase is a fine-grained mixture of anorthitic plagioclase and grossular, which is probably an alteration product of melilite.
16. Olivine in these chondrules is very Mg-rich [Mg number (Mg#) = 99.3 for both of two], which is comparable to those in OIs, but its oxygen isotopic composition (measured only for Y86009-F) is much less anomalous than the latter, indicating that Mg# alone cannot be a measure of the degree of oxygen isotopic anomalies.
17. J. A. Wood and A. Hashimoto, *Geochim. Cosmochim. Acta* **57**, 2377 (1993).
18. D. D. Clayton and co-workers proposed a different model, in which refractory interstellar dust may have longer lifetimes and may retain "cosmic chemical memory" of the earlier stage of galactic chemical evolution, resulting in ~5% excess in ^{16}O on average [K. Liffman and D. D. Clayton, *Proc. Lunar Planet. Sci. Conf.* **18**, 657 (1988); D. D. Clayton, *Astrophys. J.* **334**, 191 (1988); ______, P. Scowmen, K. Liffman, *ibid.* **346**, 531 (1989)]. However, this model may also have difficulties in explaining the uniqueness of the oxygen isotopic anomalies observed in various objects, especially similar anomalies both inside and on the rims of CAIs (*19*).
19. L. R. Nittler, in *Astrophysical Implications of the Laboratory Study of Presolar Materials*, T. Bernatowicz and E. Zinner, Eds. (American Institute of Physics, Woodbury, NY, 1997), pp. 59–82.
20. L. R. Nittler, C. M. O'D. Alexander, J. Wang, X. Gao, *Nature* **393**, 222 (1998).
21. H. Hiyagon, *Lunar Planet. Sci.* **XXIX**, abstr. no. 1582 (1998).
22. Wark-Lovering rims are sequences of mineralogically distinct layers enclosing CAIs with total thickness of ~50 μm [D. A. Wark and J. F. Lovering, *Proc. Lunar Planet. Sci. Conf.* **8**, 95 (1977); G. J. MacPherson, L. Grossman, J. M. Allen, J. R. Beckett, *ibid.* **12**, 1079 (1981)].
23. K. D. McKeegan, L. A. Leshin, G. J. MacPherson, *Meteorit. Planet. Sci. Suppl.* **32**, abstr. no. 5254 (1998); see also (*16*).
24. Accretionary rims are layers of fine-grained materials mantling CAIs that are most notable at their topographic depression [G. J. MacPherson, A. Hashimoto, L. Grossman, *Geochim. Cosmochim. Acta* **49**, 2267 (1985)].
25. R. G. Prinn and B. Fegrey Jr., in *Origin and Evolution of Planetary and Satellite Atmospheres*, S. K. Atrea, J. B. Pollack, M. S. Matthews, Eds. (Univ. of Arizona Press, Tucson, AZ, 1989), pp. 78–164.
26. R. N. Clayton, N. Onuma, T. K. Mayeda, *Earth Planet. Sci. Lett.* **30**, 10 (1976). R. N. Clayton, *Ann. Rev. Earth Planet. Sci.* **21**, 115 (1993).
27. The Yamato-86009 CV3 chondrite sample was supplied by the National Institute of Polar Research, Japan. This work was financially supported in part by a Grant-in-Aid for Scientific Research from the Ministry of Education, Science and Culture, Japan (no. 09440183 to H.H.).

21 August 1998; accepted 29 December 1998

Elongation of Oligopeptides in a Simulated Submarine Hydrothermal System

Ei-ichi Imai,[1] Hajime Honda,[1] Kuniyuki Hatori,[1] André Brack,[2] Koichiro Matsuno[1]*

Oligomerization of a peptide was attempted in a flow reactor that simulated a submarine hydrothermal system. When fluid containing glycine repeatedly circulated through the hot and cold regions in the reactor, oligopeptides were made from glycine. When divalent ions (such as copper ions) were added under acidic conditions, oligoglycine was elongated up to hexaglycine. This observation suggests that prebiotic monomers could have oligomerized in the vicinity of submarine hydrothermal vents on primitive Earth.

The onset of polymerization must have been a major step in the chemical evolution that formed the precursors of life (*1*–*4*). The underlying chemical reaction requires an organization in which products can be repeatedly transformed into reactants, as seen with ribosomes and ribozymes in contemporary biological organisms. Systems or processes that could have assisted the transformation of products to reactants might include heating in dry and wet conditions, the diurnal cycle, tidal waves, and dry-wet cycles in lagoons (*5*). Submarine hydrothermal vents (*6*) have been recognized as a possible environment for prebiotic synthesis; in this environment, products that were synthesized in hot vents could reenter the vents after being quenched in the surrounding cold water.

The thermal synthesis of products in hot vents (*7*) and the subsequent rapid cooling in surrounding cold water are generative and selective when combined (*8*). Thus, hydrothermal vents in the sea could have been an environment where oligomers and polymers were synthesized and selected. For instance, when two amino acid molecules form a peptide bond in hot vents and then the product is ejected into the surrounding cold water, the peptide bond could survive in the cold environment if the dissociation process [including decarboxylation, deamination, or dehydration (*9*)] is retarded.

We constructed a flow reactor that simulated the pressure and temperature conditions of the hydrothermal circulation of water in order to examine the likelihood of synthesizing oligopeptides from monomeric amino acids (*10*). However, there were still some large differences, for instance, in pH, CO_2, Na, and Cl contents. In our flow reactor (Fig. 1), a high-temperature high-pressure fluid was injected into a low-temperature chamber that was maintained at about the same high pressure as the fluid. The fluid circulated in a closed manner in the system with a fixed turnover rate. The fluid was heated and compressed in one part of the circuit; the rest of the chamber was cooled externally. Samples of the fluid were repeatedly taken from the low-temperature chamber for measurement at a given time interval, and the fluid in the low-temperature chamber was then returned into the high-temperature high-pressure fluid.

We prepared 100 mM glycine solution that was dissolved in pure water, and we maintained the total volume of the circulating fluid at 500 ml. The pressure of the high-pressure high-temperature chamber with its 15-ml volume was set at 24.0 MPa, which is only slightly higher than the pressure of the critical point of water (22.1 MPa). This pressure was chosen to maintain the water in the chamber as a liquid. The temperature of the high-temperature chamber was varied from 110° to 350°C in different runs. The results of interest were obtained for temperatures ranging roughly between 200° and 250°C. Temperature was increased gradually over 20 min. We started the measurements of the yields when the designated temperature was reached. The diameter of the nozzle from which a jet stream of high-temperature high-pressure fluid was injected into the low-temperature

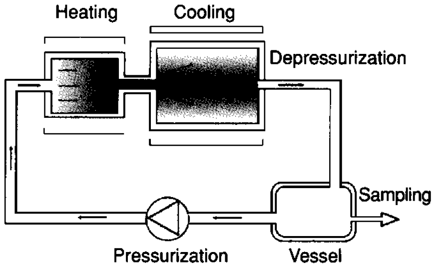

Fig. 1. A schematic drawing of a flow reactor simulating a submarine hydrothermal system.

---

[1] Department of BioEngineering, Nagaoka University of Technology, Nagaoka 940-2188, Japan. [2] Centre de Biophysique Moleculaire, CNRS, 45071 Orléans Cedex 2, France.

*To whom correspondence should be addressed. E-mail: kmatsuno@vos.nagaokaut.ac.jp